Volume 64, Issue 2, 2020
Journal of Scientific Research
Institute of Science,
Banaras Hindu University, Varanasi, India.

Enhancement of Structural, Optical and Electrical Properties of Manganese Doped Stannic Oxide Nanoparticles

G Rubyshia Santhakumari*[1], S John Kennady Vethanathan[1], and K. U. Madhu[2]

[1]Department of Physics, St. John's College, Palayamkottai- 627002, India.
(Affiliated to Manonmaniam Sundaranar University, Abishekapatti, Tirunelveli-627012, Tamilnadu, India)
grubyshia@gmail.com*, jk_glen05@yahoo.co.in
[2]Department of Physics, S. T. Hindu College, Nagercoil- 629180, India. Kmadhu71@yahoo.co.in

Abstract: **In the present study the manganese doped stannic oxide nanoparticles were synthesized by microwave assisted solution method. The structural characteristic of the synthesized nanoparticle was investigated by X-ray diffraction spectra. The particle size was estimated from the diffraction spectra data. Morphological analysis of manganese doped stannic oxide nanoparticle by scanning electron microscope. The elemental composition was confirmed by Energy dispersive X-Ray Spectroscopy. The optical band gap was determined from Ultraviolet- Visible spectroscopy. The characterization results had shown the successful doping of Manganese in the stannic oxide. Complex impedance analysis was used to predict the dominance of grain boundary resistance in the doped samples. The dielectric parameters of stannic oxide nanoparticles were reduced by increasing the concentration of manganese.**

Index Terms: **Dielectrics, manganese, nanoparticles, optical band gap, stannic oxide.**

I. Introduction

Nanometer-sized semiconductor metal oxides receive much attention due to their physical, chemical, magnetic and optical properties (Gu et al., 2004). In this study was focused on the post-transition metal oxide namely, stannic oxide (SnO_2). Tin (Sn) is a naturally occurring element that appears in group 14 of the periodic table. Tin coating provides protection against oxidation of the metal (Selamat et al., 2014). Tin oxide are used as catalysis (Eranna et al., 2004), chemical gas sensing (Jia et al., 2004), heat reflection (Song, 1999) and microelectronics (Lamelas & Reid, 1999).

The crystalline structure, size and shape of the particles depend on the method of synthesis (Jiang et al., 2008). The stannic oxide nanostructures have been synthesized by using chemical techniques rendering innovative applications (Schmidt & Helmut, 2001). The various chemical techniques are electro deposition, sol-gel technique, solvothermal and hydrothermal for the synthesis of nanoparticles. Owing to this solvothermal method was used in this present work. The heating treatment is conducted by microwave using domestic microwave oven of 2.45 GHz. Microwave method have the advantage of employing lower reaction times with respect to the other chemical methods. Microwave heating upgrades the reaction rate, significant aspect and size dissemination of nanoparticles. Microwave assisted synthesis is expeditious and cost-effective than conventional method (Gerbec et al., 2005). Manganese (Mn) is one of the transition metal is used as the doping material due to dielectric polarizability of Mn is lower than Sn. Manganese acts as a good activator to tune the optical and electrical properties of stannic oxide nanoparticles than other transition metals (Salah N, et al., 2016). The aim of this paper is to investigate the structural, optical and electrical properties of SnO_2 by doping the manganese through the characterization.

II. Experimental

A. Materials

Stannous chloride dihydrate ($SnCl_2{\cdot}2H_2O$), Manganese chloride ($MnCl_2.4H_2O$), urea and ethylene glycol were purchased from Merck was used without further purification. For the synthesis of manganese doped stannic oxide nanoparticle, $SnCl_2.2H_2O$ as a precursor, $MnCl_2.4H_2O$ as a dopant, urea as a catalyst and ethylene glycol as a solvent. All the chemicals were of analytical grade.

* Corresponding Author

B. Synthesis of Manganese doped Stannic Oxide Nanoparticle

For the synthesis of stannic oxide nanoparticle, 11.28 g $SnCl_2 \cdot 2H_2O$, and 9 g Urea was dissolved in 50 ml of Ethylene glycol under constant agitation for an hour in magnetic stirrer at room temperature. After 1 hour of stirring, the stirred solution was heated in a domestic microwave oven of 2.45 GHz at 100˚C with 540 W. At the boiling point of the solution, the urea liberates the hydroxide ions which can cause precipitation of metal oxide. The urea was decomposed slowly by maintaining steady temperature (Marinho, J. Z., et al., 2012) to control the nucleation process for yielding the controlled growth rate of SnO_2 nanoparticle. The resultant nanoparticle was collected by drying the solution up to the formation of precipitate in microwave oven. The unwanted organic impurities are removed from the precipitate by washing with double distilled water and acetone (Karpagavalli, S, et al., 2019). The resultant nanoparticles were annealed at 400ºC to get stannic oxide nanoparticle. Finally, the yield powder was grounded by using agate pestle and mortar.

For the Mn doped stannic oxide nanoparticles $MnCl_2.4H_2O$ were used as dopant. This dopant was incorporated at various weight percentages (2, 4, 6, 8 and 10). The percentage of Sn and urea remains constant and the percentage of Mn was varied throughout the nanoparticle synthesis. The final solution of different weight percentages of manganese was treated in the way as the un-doped SnO_2 nanoparticles synthesized.

III. CHARACTERIZATION TECHNIQUES

Powder X-ray Diffraction (XRD) patterns of the synthesized samples were taken by a X-ray powder diffractometer (PANalyticalX'PertPRO) with Cu Kα radiation (λ = 0.15406 nm). The scan was taken between 2θ of 20˚ and 2θ of 80˚ at increments of 0.02˚ with a count time of 4 seconds for each step. The morphology was examined using Scanning Electron Microscope and elemental composition of nanoparticles was analyzed by Energy Dispersive X-ray Analysis (SEM-EDAX, JEOL 6390LA). The absorption characteristics of the synthesized nanoparticles were investigated by diffuse reflectance spectra (Agilent Cary 5000 UV-Vis spectrometer). The impedance and dielectric measurements were carried out in the frequency range 42 Hz to 5 MHz using Soltran Dielectric Interface and Impedance Analyzer (SI 1296 and SI 1260).

IV. Results and discussion

A. Structural Properties

1) XRD Analysis

Powder X-ray diffraction spectra for manganese doped stannic oxide nanoparticle shown in the Fig. 1. Diffraction pattern reveals the crystalline structure and particle size of pure and Mn doped (2wt%, 4wt%, 6wt%, 8wt% and 10wt%) SnO_2 nanoparticles. The prominent peaks of the XRD pattern are similar to those of the standard JCPDS file no 41-1445. Fig. 1 shows the sharp diffraction peak at 26.70˚, 34.08˚, 37.99˚, 39.08˚, 51.82˚, 54.92˚, 57.97˚, 61.96˚, 64.94˚, 66.05˚, 71.28˚, 78.73˚ and confirmed the formation of tetragonal structure. FWHM and intensity of the X-ray Diffraction peaks decrease on increasing the manganese ion. The particle size of Mn doped SnO_2 nanoparticle for different concentration was calculated for the most intense diffraction peak (110) by using Scherrer formula (Patterson, 1939) denoted in (1)

$$D = \frac{K\lambda}{\beta \cos\theta} \text{ nm} \quad (1)$$

Where D is the particle size, K is the shape factor(0.94), λ is the wavelength of X-rays (λ= 1.54059 Å), β is the full width at half maximum (FWHM) and θ is the angle of diffraction. FWHM of the diffraction peaks were calculated using Origin 8 software (Lu, P. J, et al., 2015) and listed in Table. I. The lattice parameters (a,b,c) (Kasar et al., 2008) were determined using (2)

$$\frac{1}{d^2} = \frac{h^2+k^2}{a^2} + \frac{l^2}{c^2} \quad (2)$$

Where d is the interplanar spacing and h, k and l are the miller indices.

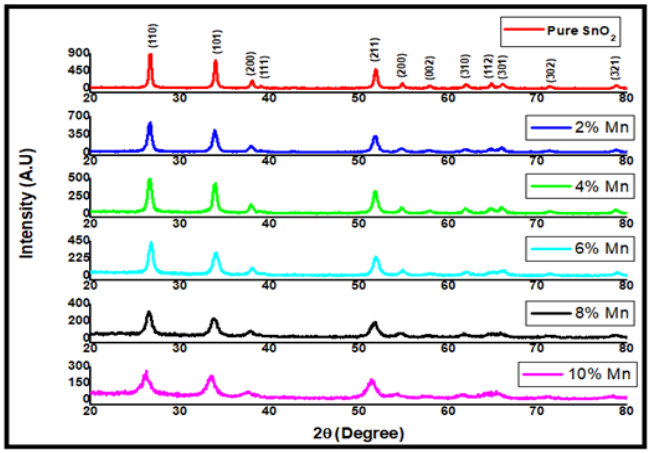

Fig. 1. XRD pattern of Mn doped SnO_2

The crystallite size, lattice constants and cell volume of Mn doped stannic oxide nanoparticles were calculated and listed in Table. I. The particle size of SnO_2 nanoparticle was decreased from 23 to 11 nm by increasing manganese concentration. By increasing the weight percentage of the dopant, the diffraction peak intensity was decreased. From Table. I it was clearly noticed that due to increasing the dopant, FWHM also increases. Thus the decrease in the lattice constants and unit cell volume of the synthesized nanoparticle is due to the ionic radius

(Cojocaru et al., 2017) of Mn^{4+} (0.53 Å) (Balaji et al., 2012) is smaller than Sn^{4+} (0.71 Å) (Yao et al., 2013).

Table I. Structural Parameters of synthesized Mn doped SnO_2

Mn %	Particle size (nm)	Lattice parameter		Volume (Å^3)	FWHM
		a=b (Å)	c (Å)		
0	27.49	4.81	3.34	77.62	0.1476
2	23.18	4.75	3.23	73.219	0.2460
4	21.28	4.74	3.21	72.326	0.2952
6	17.56	4.73	3.20	71.810	0.344
8	15.22	4.71	3.19	71.027	0.4428
10	11.34	4.70	3.19	70.705	0.7872

The particle size calculation and lattice strain was also calculated by Williamson–Hall (W–H) plot method. The broadening of XRD peaks (β_{hkl}) is the sum of size broadening (β_D) and strain broadening (β_s) (Venugopal, et al., 2014).

$$\beta_{hkl} = \beta_o + \beta_s$$

$$\beta_{hkl}\ cos\theta = \left(\frac{k\lambda}{D}\right) + 4\varepsilon_s\ sin\theta \qquad (3)$$

Where ε_S is lattice strain. The Williamson–Hall plot is a plot of β cos(θ) versus 4sin(θ). The particle size was calculated from the y-intercept of W–H plot. The slope of the straight line fit was used to obtain the lattice strain of the synthesized nanoparticles. The lattice strain will lead to a broadening in the XRD peaks (Nandan, et al., 2013). Fig. 2 shows the W–H plot of pristine and Mn doped stannic oxide nanoparticles. From the Table. II it was confirmed that the particle size was determined from the W–H plot was nearly equal to the crystallite size was calculated from the Scherrer formula The lattice strain of the synthesized nanoparticles were observed from the negative slope of the fitted lines of the W–H plot. This negative lattice strain values indicating the presence of compressive strain in the lattice of SnO_2 due to the doping of manganese. Thus the lattice strain occurrence results in the broadening of the XRD peak

2) Morphological analysis

SEM images of pure SnO_2 nanoparticle with magnification of 100 µm and 1µm are shown in the Fig. 3 and labeled as S1A and S1B. In Fig. 3 for Mn doped SnO_2 nanoparticles (2, 4, 6, 8 and 10 wt%, Mn) with magnification of 100 µm are labeled as S2A, S3A, S4A, S5A and S6A and 1µm magnification are labeled as S1B, S2B, S3B, S4B, S5B and S6B. The 1µm magnification SEM images show the spherical shape of individual nanoparticles. The nanoparticles shown in the 100 µm magnification were appeared to be porous this would be favorable for gas sensors because pores would promotes gas diffusion (Suematsu et al., 2019).

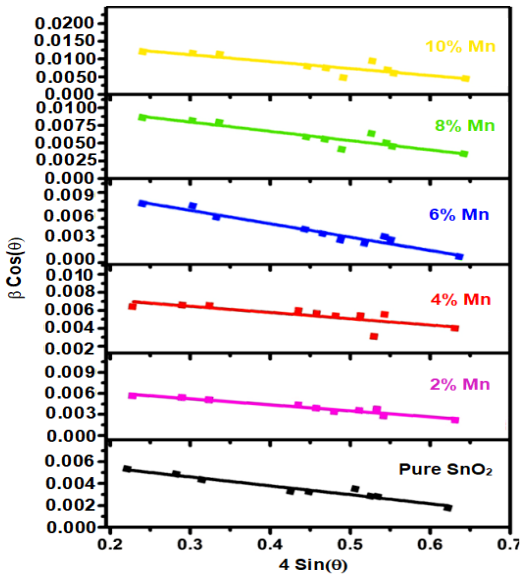

Fig. 2. Williamson–Hall Plot of Pristine and Mn doped stannic oxide nanoparticle

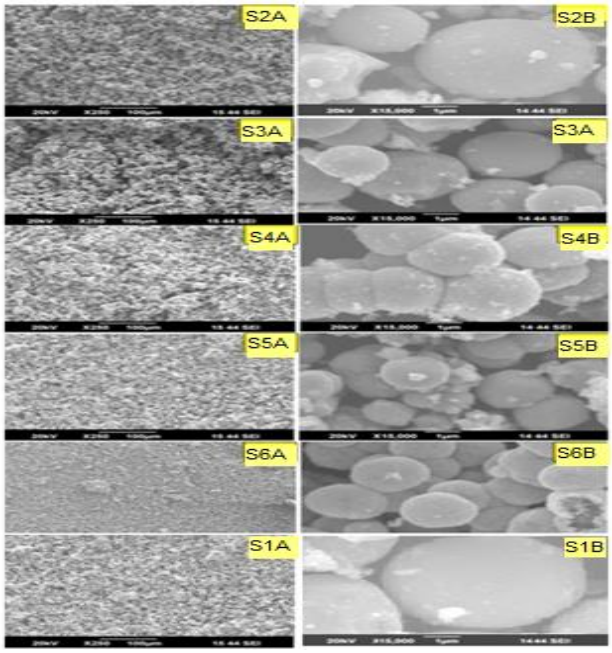

Fig. 3. SEM image of Mn doped SnO_2 nanoparticle with magnification of 100 µm and 1 µm

The SEM image clearly shows that the particle size of synthesized nanoparticles decrease significantly with increasing manganese concentration. This is due to the ionic radius of Mn^{4+} is smaller than Sn^{4+}. Sn ions had been replaced by Mn ions due to doping the manganese in controlled manner into stannic oxide lattice.

Table II. W-H Plot - Structural parameters of Pure and Mn doped SnO_2

Mn %	Particle size (nm)	Lattice strain
0	25.33	-0.00571
2	22.09	-0.009375
4	19.35	-0.00625
6	16.18	-0.02
8	13.92	-0.00892
10	10.16	-0.00365

3) Elemental compositional analysis

EDX spectrum of pristine and Mn doped stannic oxide nanoparticles (2, 4, 6, 8 and 10 wt%, Mn) are shown in the Fig. 4 and labeled as E1, E2, E3, E4, E5 and E6. The presence of tin, manganese and oxygen element in Mn doped stannic oxide nanoparticle was confirmed by the EDX spectrum. The weight percentages of Sn, Mn and oxygen atom were reported in the Table. III.

Table III. Elemental composition of Mn doped SnO_2

Mn %	Element	Wt %	At %
0	O	24.2	70.32
	Sn	75.8	29.68
2	O	26.80	72.52
	Sn	71.36	26.03
	Mn	1.84	1.45
4	O	27.87	72.98
	Sn	68.31	24.11
	Mn	3.82	2.91
6	O	29.32	73.39
	Sn	63.62	21.46
	Mn	7.06	5.15
8	O	30.4	74.08
	Sn	61.58	20.23
	Mn	8.02	5.69
10	O	32.36	75.25
	Sn	58.5	18.13
	Mn	9.14	6.62

B. Optical Properties

Fig. 5 reveals the diffuse reflectance spectrum of manganese doped stannic oxide nanoparticles. As a result of absorption, the reflectance of stannic oxide nanoparticles shows the peak around 280 to 400 nm. There is a significant shift in the reflectance spectrum with increasing Mn concentration.

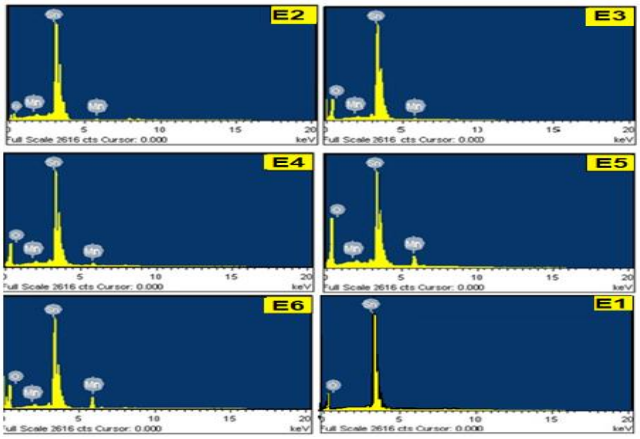

Fig. 4. EDX spectra of Pristine and Mn doped stannic oxide nanoparticle

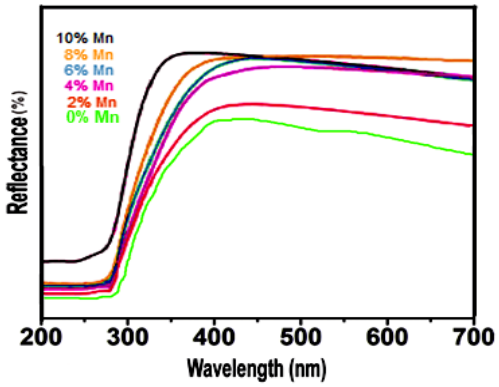

Fig. 5. UV–Visible diffuse reflectance spectra of Mn doped SnO_2 nanoparticles

The reflectance spectra was assayed using the Kubelka-Munk relation (Pal, M, et al., 2012)

$$F(R) = (1-R)^2 / 2R \quad (4)$$

Where F(R) = α is the K–M function and R is the percentage of reflectance. Equation (5) is used to correlate the absorption coefficient (α) and optical band gap E_g (Ghobadi, 2013)

$$\alpha h\upsilon = A(h\upsilon - E_g)^n \quad (5)$$

Where A is absorbance, E_g is the optical band gap energy and h is Planck's constant. The exponent n varies according to allowed direct, allowed indirect, forbidden direct or forbidden indirect transitions and the values are 1/2, 2, 3/2 and 3 (Viezbicke et al., 2015).

For stannic oxide nanoparticles, n depends on the allowed direct transition (Selvakumari et al., 2017). E_g of the pure and Mn doped SnO_2 nanoparticles was obtained using Tauc's method (Suram et al., 2016). Thus the band gap energy can be

determined by plotting $(F(R)\ h\upsilon)^2$ versus $h\upsilon$. Fig. 6 shows the tauc plot of stannic oxide nanoparticles.

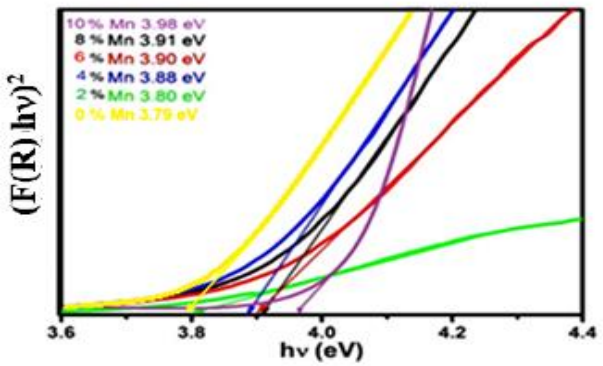

Fig. 6. Tauc plot of Mn doped SnO_2 nanoparticles

Table. IV reveals that E_g value of stannic oxide nanoparticles is enhanced by increasing the manganese concentration and results in blue shift from the bulk SnO_2 of 3.6 eV (Zhou et al., 2014). This is due to lattice strain (Nandan, et al., 2013) with the decrease of particle size for increasing manganese concentration in stannic oxide nanoparticle.

Table IV. Band gap values for different Mn concentration

Dopant concentration Mn %	**Band gap energy, E_g (eV)**
0	3.79
2	3.80
4	3.88
6	3.90
8	3.91
10	3.98

C. Electrical Properties

1) Dielectric Constant

Fig. 7 shows the variation of dielectric constant of Pristine and Mn doped stannic oxide nanoparticles with respect to the frequency (42 Hz – 5 MHz) at room temperature.

The dielectric polarizability of manganese ions (2.64 $Å^3$) is smaller than tin ions (2.84 $Å^3$) (Shannon & Robert, 1993). Thus the dielectric constant of stannic oxide nanoparticle decreases as the concentration of manganese increases as revealed from the Fig. 7. The dielectric constant decreases as the frequency of the applied field increases and becomes constant at high frequency for all concentrations of manganese. For pure SnO_2, dielectric constant becomes constant beyond 794 kHz frequency and Mn doped SnO_2 nanoparticles remains constant after 3.16 kHz frequency.

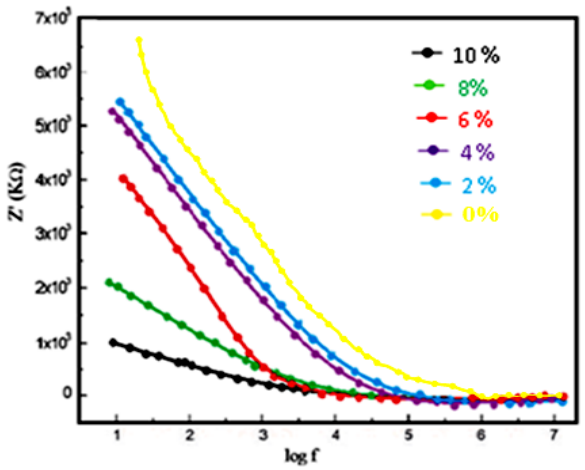

Fig. 7. Variation of dielectric constant with frequency

2) Dielectric Loss (tan δ)

Fig. 8 shows the loss tangent exhibits behavior similar to the dielectric constant and also the synthesized nanoparticles show no loss peak. Due to high resistivity, dielectric loss attains high at low frequency region. Thus the manganese doped stannic oxide nanoparticle can be used in high frequency microwave devices (Azam et al., 2010).

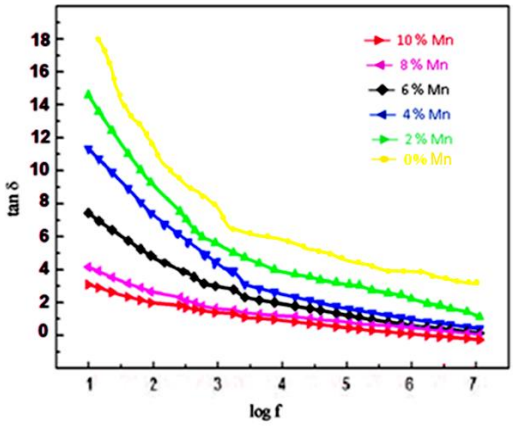

Fig. 8.Dielectric loss varies with frequency

3) AC Conductivity

Fig. 9 shows the AC conductivity of Mn doped stannic oxide nanoparticle varies with frequency at room temperature. The conductivity gradually increases at low frequency but increases rapidly at high frequency. Therefore increasing the manganese concentration impedes the flow of charge carriers in stannic oxide nanoparticles (Azam et al., 2010). This results the conductivity of the system is decreased.

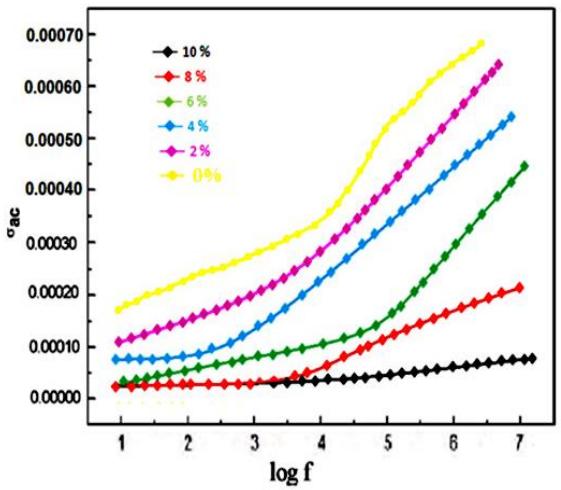

Fig. 9. AC conductivity varies with frequency

4) Impedance Analysis

The AC Complex Impedance Spectroscopy (CIS) technique is used to obtain the electrical parameters of manganese doped stannic oxide nanoparticles (Maldonado et al., 2014). The CIS data contains the resistive and capacitive components of the synthesized nanoparticles which are analyzed using the Nyquist plot is shown in the Fig. 10. It is clear that all the doped stannic oxide nanoparticles show single semicircular arc.

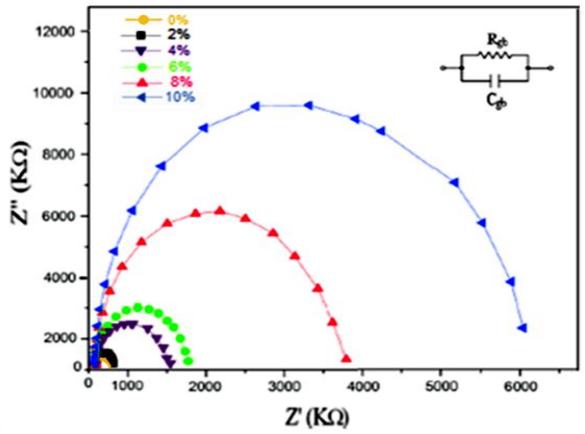

Fig. 10. Nyquist plot for Mn doped stannic oxide nanoparticle at room temperature

The equivalent electrical circuit is shown in the inset of Fig. 10 used to represent the electrical properties of the sample is obtained from Z-view software. The value of grain boundary resistance (R_{gb}) and grain boundary capacitance (C_{gb}) was tabulated in Table V.

On doping the manganese in to SnO_2, the values of grain boundary resistance increased and grain boundary capacitance decreased. Thus the grain boundary contribution is increased (Mehraj et al., 2013) and results in only one semi-circular arc for different concentration of manganese doped stannic oxide nanoparticle. Thus the crystallite size decreases on doping manganese into the stannic oxide lattice, the grain boundary contribution was dominated (Takaki et al., 2014). Due to the grain boundary resistance it can be suited for resistance based gas sensor device at room temperature (Deb, B., et al., 2007).

Table V. Values of electrical parameter for different Mn concentration

Dopant concentration %	**R_{gb} (KΩ)**	**C_{gb} (nF)**
0	72.518	1.10256
2	2567.4	0.06723
4	4528.9	0.03736
6	12319.3	0.03234
8	18643.1	0.03095
10	63429.7	0.02801

CONCLUSION

Mn doped SnO_2 nanoparticles were successfully synthesized using microwave assisted solution method. The structural, morphological, optical and impedance properties for manganese doped stannic oxide nanoparticle was studied. The particle size of SnO_2 nanoparticle was decreased by increasing the weight percentage of manganese. This is because the ionic radius of manganese is smaller than that of stannum. The synthesized sample shows spherical in shape and the doping of manganese in SnO_2 lattice is confirmed through EDAX spectrum. Complex impedance spectrum shows one semicircular arc for all dopant concentration of manganese indicating the grain boundary contribution.

REFERENCES

Azam, A., Ahmed, A. S., Chaman, M., & Naqvi, A. H. (2010). Investigation of electrical properties of Mn doped tin oxide nanoparticles using impedance spectroscopy. *Journal of Applied Physics*, 108(9), 094329.

Balaji, S., Manichandran, T., & Mutharasu, D. (2012). A comprehensive study on influence of Nd^{3+} substitution on properties of $LiMn_2O_4$. *Bulletin of Materials Science*, 35(3), 471-480.

Cojocaru, B., Avram, D., Kessler, V., Parvulescu, V., Seisenbaeva, G., & Tiseanu, C. (2017). Nanoscale insights into doping behavior, particle size and surface effects in trivalent metal doped SnO_2. *Scientific reports*, 7(1), 1-14.

Deb, B., Desai, S., Sumanasekera, G. U., & Sunkara, M. K. (2007). Gas sensing behaviour of mat-like networked tungsten oxide nanowire thin films. *Nanotechnology*, *18*(28), 285501.

Eranna, G., Joshi, B. C., Runthala, D. P., & Gupta, R. P. (2004). Oxide materials for development of integrated gas sensors—a comprehensive review. *Critical Reviews in Solid State and Materials Sciences*, 29(3-4), 111-188.

Gerbec, J. A., Magana, D., Washington, A., & Strouse, G. F. (2005). Microwave-enhanced reaction rates for nanoparticle synthesis. *Journal of the American Chemical Society*, 127(45), 15791-15800.

Ghobadi, N. (2013). Band gap determination using absorption spectrum fitting procedure. International Nano Letters, 3(1), 2.

Gu, F., Wang, S. F., Lü, M. K., Zhou, G. J., Xu, D., & Yuan, D. R.(2004). Photoluminescence properties of SnO_2 nanoparticles synthesized by sol− gel method. *The Journal of Physical Chemistry B*, 108(24), 8119-8123.

Jia, Z. J., Zhu, L. P., Liao, G. H., Yu, Y., & Tang, Y. W. (2004). Preparation and characterization of SnO nanowhiskers. *Solid state communications*, 132(2), 79-82.

Jiang, J., Oberdörster, G., Elder, A., Gelein, R., Mercer, P., & Biswas, P. (2008). Does nanoparticle activity depend upon size and crystal phase?. *Nanotoxicology*, 2(1), 33-42.

Karpagavalli, S., Vethanathan, S. J. K., & Perumal, S. (2019). Asian JournaL of Chemistry. *Asian Journal of Chemistry*, *31*(4), 793-798.

Kasar, R. R., Deshpande, N. G., Gudage, Y. G., Vyas, J. C., & Sharma, R. (2008). Studies and correlation among the structural, optical and electrical parameters of spray-deposited tin oxide (SnO_2) thin films with different substrate temperatures. *Physica B: Condensed Matter*, 403(19-20), 3724-3729.

Lamelas, F. J., & Reid, S. A. (1999). Thin-film synthesis of the orthorhombic phase of SnO_2. *Physical Review B*, 60(13), 9347.

Lu, P. J., Huang, S. C., Chen, Y. P., Chiueh, L. C., & Shih, D. Y. C. (2015). Analysis of titanium dioxide and zinc oxide nanoparticles in cosmetics. *Journal of food and drug analysis*, *23*(3), 587-594.

Maldonado, K. L., De La Presa, P., De La Rubia, M. A., Crespo, P., De Frutos, J., Hernando, A., ... & Galindo, J. E. (2014). Effects of grain boundary width and crystallite size on conductivity and magnetic properties of magnetite nanoparticles. *Journal of nanoparticle research*, 16(7), 2482.

Marinho, J. Z., Romeiro, F. C., Lemos, S. C. S., Motta, F. V., Riccardi, C. S., Li, M. S., ... & Lima, R. C. (2012). Urea-based synthesis of zinc oxide nanostructures at low temperature. *Journal of Nanomaterials*, *2012*.

Mehraj, S., & Ansari, M. S. (2013). Structural, dielectric and complex impedance properties of Cd doped SnO_2 nanoparticles. *Journal of Nanoengineering and Nanomanufacturing*, 3(3), 229-236.

Nandan, B., Venugopal, B., Amirthapandian, S., Panigrahi, B. K., & Thangadurai, P. (2013). Effect of Pd ion doping in the band gap of SnO_2 nanoparticles: structural and optical studies. *Journal of nanoparticle research*, *15*(10), 1999.

Pal, M., Pal, U., Jimenez, J. M. G. Y., & Perez Rodriguez, F. (2012). Effects of crystallization and dopant concentration on the emission behavior of TiO_2:Eu nanophosphors. *Nanoscale research letters*, *7*(1), 1-12.

Patterson, A. L. (1939). The Scherrer formula for X-ray particle size determination. *Physical review*, 56(10), 978.

Salah, N., Habib, S., Azam, A., Ansari, M. S., & Al-Shawafi, W. M. (2016). Formation of Mn-doped SnO_2 nanoparticles via the microwave technique: structural, optical and electrical properties. *Nanomaterials and Nanotechnology*, *6*, 17.

Schmidt, H. (2001). Nanoparticles by chemical synthesis, processing to materials and innovative applications. *Applied organometallic chemistry*, 15(5), 331-343.

Selamat, M. Z., Masron, F., Yusuf, M., Yusri, M., Kamarolzaman, A. A., Mohd Tahir, M., & Herawan, S. G. (2015). Effect of stannum on properties of graphite/stannum composite for bipolar plate. *In Applied Mechanics and Materials* (Vol. 699, pp. 157-162).

Selvakumari, J. C., Ahila, M., Malligavathy, M., & Padiyan, D. P. (2017). Structural, morphological, and optical properties of tin (IV) oxide nanoparticles synthesized using Camellia sinensis extract: a green approach. *International Journal of Minerals, Metallurgy, and Materials*, 24(9), 1043-1051.

Shannon, R. D. (1993). Dielectric polarizabilities of ions in oxides and fluorides. *Journal of Applied physics*, 73(1), 348-366.

Song, S. K. (1999). Characteristics of SnO_x films deposited by reactive-ion-assisted deposition. *Physical Review B*, 60(15), 11137.

Suematsu, K., Uchino, H., Mizukami, T., Watanabe, K., & Shimanoe, K. (2019). Oxygen adsorption on ZrO_2-loaded SnO_2 gas sensors in humid atmosphere. *Journal of materials science*, 54(4), 3135-3143.

Suram, S. K., Newhouse, P. F., & Gregoire, J. M. (2016). High throughput light absorber discovery, part 1: an algorithm for automated tauc analysis. *ACS combinatorial science*, 18(11), 673-681.

Takaki, S., Akama, D., Nakada, N., & Tsuchiyama, T. (2014). Effect of grain boundary segregation of interstitial elements on Hall–Petch coefficient in steels. *Materials Transactions*, 55(1), 28-34.

Venugopal, B., Nandan, B., Ayyachamy, A., Balaji, V., Amirthapandian, S., Panigrahi, B. K., & Paramasivam, T. (2014). Influence of manganese ions in the band gap of tin oxide nanoparticles: structure, microstructure and optical studies. *RSC Advances*, *4*(12), 6141-6150.

Viezbicke, B. D., Patel, S., Davis, B. E., & Birnie III, D. P. (2015). Evaluation of the Tauc method for optical absorption edge determination: ZnO thin films as a model system. *physica status solidi (b)*, 252(8), 1700-1710.

Yao, X., Yu, Q., Ji, Z., Lv, Y., Cao, Y., Tang, C, & Chen, Y. (2013). A comparative study of different doped metal cations on the reduction, adsorption and activity of $CuO/Ce_{0.67}M_{0.33O2}$ (M= Zr^{4+}, Sn^{4+}, Ti^{4+}) catalysts for NO^+ CO reaction. *Applied Catalysis B: Environmental*, 130, 293-304.

Zhou, C., Yu, J., Qin, Y., & Zheng, J. (2012). Grain size effects in polycrystalline gold nanoparticles. *Nanoscale*, 4(14), 4228-4233.

Zhou, W., Liu, Y., Yang, Y., & Wu, P. (2014). Band gap engineering of SnO2 by epitaxial strain: experimental and theoretical investigations. *The Journal of Physical Chemistry C*, 118(12), 6448-6453.

***